Faraday
Discussions

Accepted Manuscript

**Faraday
Discussions**

**Royal Society of
Chemistry**

ROYAL SOCIETY
OF CHEMISTRY

ROYAL SOCIETY
OF CHEMISTRY

www.rsc.org/faraday_d

Selective TERS Detection and Imaging through Controlled Plasmonics

Hao Wang,[1] Stacey L. Carrier,[1] Sheldon Park,[2] and Zachary D. Schultz[1]*

1. University of Notre Dame Department of Chemistry and Biochemistry, Notre Dame, IN 46530 USA
2. University of Buffalo, Department of Chemical and Biological Engineering, Buffalo, NY 14260 USA

*corresponding authors email: Schultz.41@nd.edu

ABSTRACT:

Enhanced Raman spectroscopy offers capabilities to detect molecules in the complex molecular environments and image chemical heterogeneity in a wide range of samples. It has been shown that plasmonic interactions between a TERS tip and a metal surface produce significant enhancements. In this report we show how SERS spectra from purified molecules can be used to selectively image proteins on surfaces and in cell membranes. The SERS response from the purified protein can be used to create a multivariate regression model that can be applied to nanoparticles that bind to protein receptors. Filtering the observed TERS spectra with the regression model can then selectively image the protein receptor. Experiments with mutant proteins suggest that key amino acids provide significant contributions to the observed TERS signal, which enables differentiating protein receptors. These results demonstrate the selectivity that can be obtained in TERS images through a controlled plasmonic interaction. This approach has further implications for identifying membrane receptors that bind specific molecules relevant to drug targeting and chemical signaling.

INTRODUCTION

Control of localized surface plasmon resonances has opened new avenues to high sensitivity spectroscopic detection.[1, 2] The enhancement in Raman scattering, known as surface-enhanced Raman scattering (SERS), is strongly correlated with the plasmonic properties of nanostructures.[3] Understanding of the electric fields and observed enhancements has enabled high sensitivity spectroscopic and imaging applications.[4-6]

Tip-enhanced Raman scattering (TERS), utilizes a nanostructure on the apex of scanning tunneling (STM), or atomic force (AFM), microscope tip to correlate Raman signals with nanometer spatial resolution.[7, 8] In order to obtain high sensitivity TERS detection, the tip must be in close proximity to a metal surface and generate a gap plasmon resonance mode.[9] The interaction between the plasmon resonance on the tip and plasmon in the metal surface combine to generate significant enhancements in the Raman scattering. The enhancements observed in gap resonance modes are similar to the enhancements associated with gaps between nanoparticles, commonly known as hotspots, in SERS.[10]

This high sensitivity, high spatial resolution microscopy suggests possibilities to explore complex and chemically heterogeneous systems. The observed Raman scattering provides unique opportunities to identify various molecular species and distinguish minute compositional and structural alterations. Indeed TERS has been reported from cell membranes, however the signals arising from only the tip require longer acquisition times.[11-13] Examining intact cells to study membrane receptors or lipid domains is challenging. Obtaining gap-mode like enhancements on cell membranes could address these challenges.

It has been demonstrated that enhancements comparable to those in gap modes can be achieved when a TERS tip interacts with a nanoparticle.[14] Control of the polarization can increase the spatial resolution of this interaction to the size of nanoparticle being detected.[15] Intriguingly, experiments with ligand-functionalized nanoparticles interacting with proteins on a surface give rise to Raman signals associated with the protein on the surface preferentially to the ligand on the nanoparticle probe.[16, 17] Recently, peptide functionalized nanoparticles were used to selectively detect the Raman spectrum of a protein receptor within an intact cellular membrane.[18] This selective detection indicates that Raman scattering of molecules near the nanoparticle probe, but not in the gap junction, can be selectively enhanced in TERS imaging. Interestingly, the spectrum obtained from the tip coupling to the nanoparticle in intact cell membranes is significantly different than that observed from aggregated nanoparticles on the membrane, emphasizing the importance of a controlled interaction.[18]

Previous work suggests that plasmon modes in interacting dimers can generate substantial electric fields outside the gap junction.[19] Additionally, the scattering from a molecule outside of the gap junction was predicted to show increased scattering, [20] which has been observed experimentally using super-resolution SERS imaging approaches.[21] Interestingly, recent work suggests that when the nanostructures are within 1 nm of each, quantum tunneling can alter the electric field in the gap junction and redistribute the electric field around the interacting nanostructures.[22, 23]

The origin of this selective enhancement appears to arise from the controlled interaction of the TERS tip with the nanoparticle probe. It has been shown that the plasmon modes observed from interacting nanostructures are sensitive to the spacing and orientation of the nanostructures as well as the polarization of the incident and emitted electromagnetic radiation.[24-26] Furthermore, the observed SERS spectrum is strongly dependent upon nanoparticle spacing and orientation.[27, 28]

In this report we use statistical analysis to correlate the enhanced Raman signals observed in SERS of aggregated nanoparticles with TERS detection of nanoparticle probes. The TERS experiments provide a controlled plasmonic interaction that is sensitive to molecules in and outside the gap junction. In experiments of protein receptors binding to ligands, details of conformational changes associated with these events can be reflected in the vibrational spectrum. Our results demonstrate the utility of chemometric analysis in identifying specific molecules based on statistical similarity between each spectrum in a TERS map to the reference SERS spectrum of a pure component. In particular we observe that the SERS response from purified molecules can be used to identify that molecule in the complex chemical matrix of a cell membrane by TERS. Using mutant proteins, we are further able to validate this unprecedented selectivity. The improved image contrast enables us to examine the plasmonic enhancements responsible for the signals observed in TERS experiments.

EXPERIMENTAL METHODS

Reagents. Gold nanoparticles (GNP) and microscope slides functionalized with either biotin or streptavidin were purchased from Nanocs (New York, NY). Citrate stabilized GNP spheres (NanoXact™) were purchased from nanoComposix (San Diego, CA). Short peptides with the sequence of cRGDfC were synthesized by Peptide International (Louisville, KY). Purified human integrin $\alpha_v\beta_3$ protein was purchased from Chemicon, Temecula, CA (CC1021, EMD Millipore Corporation). Coverslips used in cell culture were poly-D-lysine coated to enhance cell attachment and spreading (BD BioCoat Cellware, BD Biosciences, San Jose, CA). Paraformaldehyde was purchased from Sigma-Aldrich (St. Louis, MO). All these chemicals were used without any further purification. Ultrapure water (18.2 MΩ·cm resistivity) was obtained from a Barnstead Nanopure filtration system.

Recombinant Streptavidin Mutants. Streptavidin mutants (M5, TMC, RC) and a wild type (WT) control were expressed, extracted, and purified from *Escherichia coli* T7 Express *lys*Y competent cells with mutant plasmids and transformants on LB plates as previously reported.[29] All three mutants construct, as well as the wild type control, contain a FLAG tag (DYKDDDDK) and a six-His tag for affinity purification. These streptavidin mutants (M5, 2.14 mg/mL; TMC, 1.68 mg/mL; RC, 1.61 mg/mL; WT, 1.45 mg/mL) were dissolved in PBS for further use. Details about the amino acid mutations for these mutants can be found in Table 1.

3

Preparation of TERS sample. The first set of TERS sample was prepared by drop depositing 20~50 μL biotinylated GNP colloid of appropriate concentration (0.05%) onto streptavidin-coated slide or streptavidin derivatized GNP onto biotin functionalized slide. The slide was rinsed with ultrapure water to remove physisorbed or weakly bound GNP on the functional slide.

TERS samples with recombinant streptavidin (M5, TMC, RC, WT) were made by depositing biotinylated GNPs onto recombinant streptavidin coated slides. The derivatization of glass slide with recombinant streptavidin was processed by first cleaning the slides for 1.5 hours in acid bath, followed by rinsing with ultrapure H_2O and EtOH. After being dried, the slides were soaked in 1% (3-Glycidyloxypropyl)trimethoxysilane ethanoic solution, then rinsed repeatedly in ultrapure H_2O and finally soaked in the respective recombinant protein solutions overnight.

Figure 1 shows the observed dark field scattering and representative AFM images observed from a sample prepared on glass slides. From these images, single and aggregated particles are readily discerned.
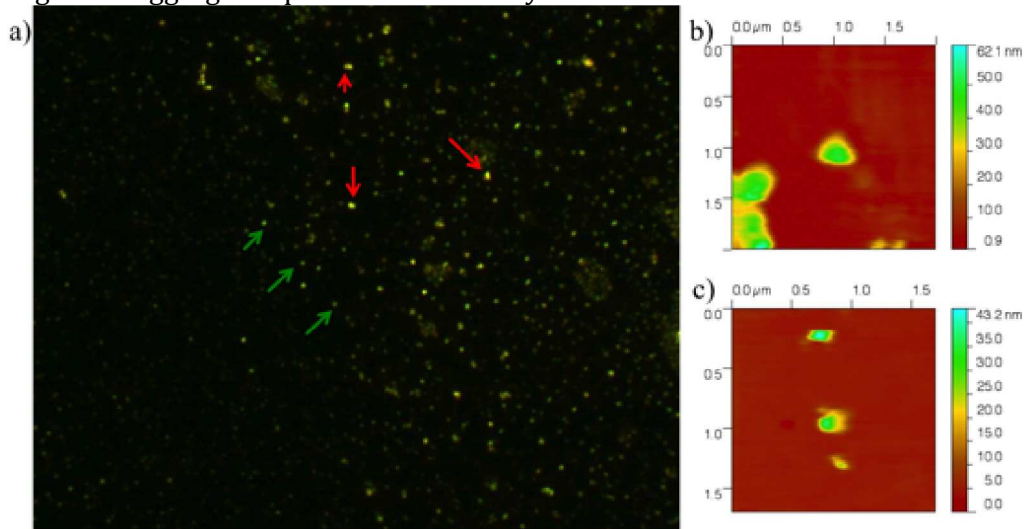
Figure 1. a) Representative dark-field image of 50 nm biotinylated GNPs deposited on streptavidin functionalized glass slide, red arrows point to bigger particles, multi-mers or clusters with bright yellow scattering and green arrows point to dim blue-greenish scattering spots for isolated single particles; b) A representative AFM image of 80 nm biotin GNPs on streptavidin slide surface is shown; c) The AFM image shows a 50 nm biotin GNPs on streptavidin slide surface.

The other set of TERS sample was prepared by culturing cyclic RGD short peptide (cRGDfC) functionalized GNPs with colon cancer cells (SW620) plated on microscope coverslips. Rinsing and fixation of the cells with 4% (w/v) paraformaldehyde were carried out followed by a rinsing step with ultrapure H_2O to remove the residual fixatives. Figure S1 (supporting information) shows the distribution of cRGDfC NPs on cells and the observed AFM topography.

Preparation of SERS sample. Functionalized GNPs with biotin and streptavidin were pelleted through centrifugation. These pellets were re-dispersed in a microliter volume of ultrapure water and drop-coated on a clean microscope slide and then covered with a glass cover slip to avoid contamination during SERS measurement. Similarly, the RGD peptide modified GNPs were incubated with purified human integrin $\alpha_v\beta_3$ protein and then pelleted, re-dispersed and drop-coated onto a glass slide for SERS.

TERS spectroscopy. TERS was performed on a combined AFM-Raman instrument composed of a commercial atomic force microscope (Nanonics MV4000 AFM) and a homebuilt Raman spectrometer. The TERS signal was collected in a top-illumination geometry (normal incidence). A 632.8 nm HeNe laser (Melles Griot) was used for excitation. The intensity and polarization of laser was controlled using a half-waveplate and polarizer. A liquid-crystal mode converter (ARCoptix, Neuchatel, NE, Switzerland) was used to generate a radial polarization, which has been shown to increase TERS contrast.[30, 31] A long working distance dark-field objective (50x, NA=0.5, LMPlanFLN, Olympus) was used to both focus the excitation and collect the scattered light from the TERS tip. The TERS tips were chemical-mechanical-polished (CMP) Au nanoparticle AFM tips (Nanonics Supertips Ltd.) with a diameter of ca. 100-200 nm. The Laser power was adjusted to be 1 mW or less at the sample to avoid damage in all experiments. The collected Raman scattering was filtered through a dichroic beamsplitter (RazorEdge, Semrock, 633 nm) and a long pass filter (RazorEdge, Semrock, 633 nm), focused onto the 50 μm entrance slit of an imaging spectrograph (Horiba, Jobin Yvon), dispersed by a 600 g/mm grating (centered at 1600 cm^{-1}), and detected with CCD camera (Horiba, Synapse).

TERS maps were obtained by scanning the sample stage under the TERS tip positioned in the laser focus. The acquisition time was 1s per pixel. The tip position and status were checked after each mapping experiment to exclude cases when the tip either drifts out of the laser focus or is contaminated.

Raman spectroscopy. SERS spectra were collected using a home-built confocal Raman microscope with a 632.8 nm HeNe laser used as the excitation source. Sample illumination was achieved through a 50x (LMPlanFLN, Olympus) dark field objective. The laser power was kept at 1 mW. The SERS spectra for biotin and streptavidin were taken from different spots on the prepared SERS nanoparticle film, with an acquisition time of 1s per spectrum in all cases.

Chemometric Analysis. Multivariate analysis was performed using PLS Toolbox (Eigenvector Research Inc., Wenatchee, WA, Version 7.0.2) working in a MATLAB R2011b (The Mathworks Inc, Natick, MA). All raw SERS and TERS spectra were preprocessed through a weighted least squares (WLS, whittaker filter, 2nd order polynomial) automatic baseline subtraction to remove the offset differences due only to the background in each spectrum. These data were further used to decompose the pure components through analysis of the SERS data using multi-variant curve resolution (MCR). Classification analysis was performed using partial least-squares discriminate analysis (PLS-DA) on the obtained SERS and TERS datasets in order to determine the class of each spectrum in the TERS map. TERS maps and score maps were reconstructed in MATLAB according to single-peak intensities and PLS-DA scores, respectively.

RESULTS AND DISCUSSION
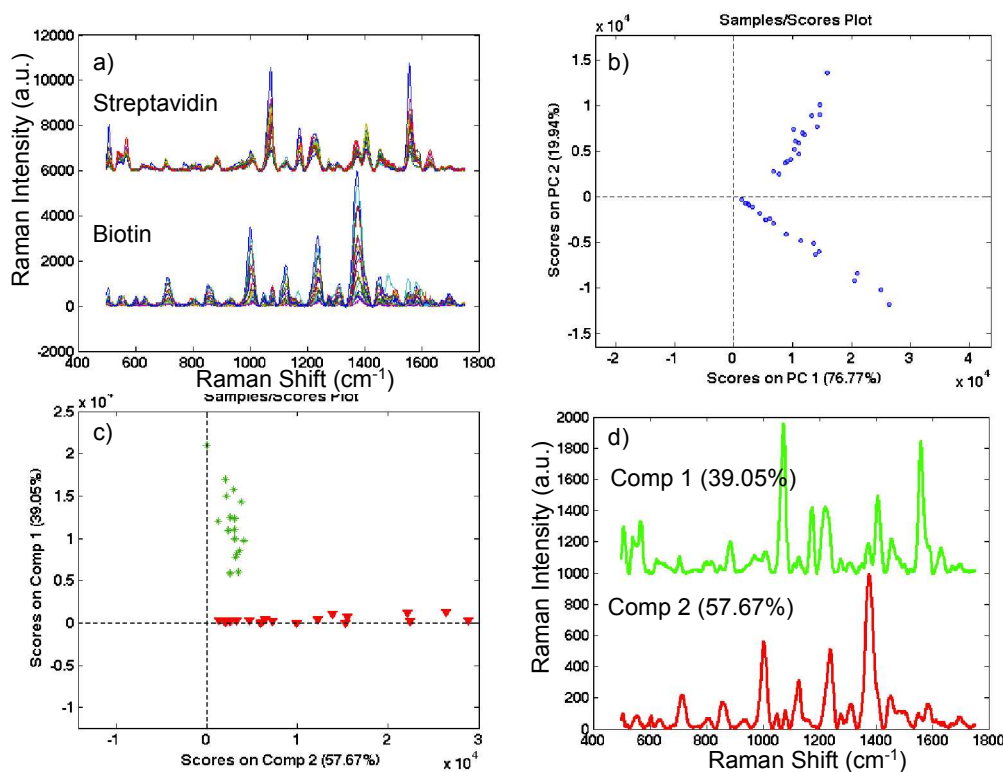
Figure 2. a) SERS spectra of pure streptavidin and biotin; **b)** sample/scores plot along two principle components in PCA analysis of the SERS data without any constraints; **c)** sample/scores plot in MCR analysis of the SERS data with non-negativity requirement and constrained number of components (2); and **d)** MCR calculated pure components from the SERS data are shown. Green and red correspond to component 1 and 2, respectively.

To identify the enhanced Raman signal of a protein bound to a ligand functionalized nanoparticle, we obtained the SERS spectra from biotinylated and streptavidin functionalized GNPs. Figure 2a shows the SERS spectra of biotin and streptavidin in aggregated GNPs. SERS spectra from each molecule are shown to have a high degree of reproducibility, showing consistent frequencies. There is variation in the absolute intensities. These spectra provide a reference to distinguish the signals from biotin and streptavidin. Figure 2b shows that principle component analysis (PCA) of the spectra in Figure 2a displays the clear, orthogonal separation expected of two components. Using constraints, associated with MCR analysis, we are able to determine orthogonal loadings that match the observed spectra as shown in Figure 2c and 2d. The score on a specific loading can be used to infer concentration information with respect to each component, providing chemically interpretable results. In this controlled data set, multivariate analysis accurately captures each chemical component.

It has been shown that chemometric analysis can be used to identify spectrally similar features within the obtained images.[11] Vibrational spectroscopic maps are commonly produced by plotting the intensity of a single frequency over the measured region. While this is straightforward and useful in a wide range of systems where unique marker band can be identified for specific components. Raman tags, for example, have been exploited due to their strong Raman response and characteristic spectral features.[32] Apart from Raman tags,

6

using a single marker band intensity is often problematic because the molecules share vibrational frequencies. Additionally, the intrinsic Raman signal of biomolecules is weak and depends on the conformation and structure of the molecule that can vary across a sample.

The reduction of data dimensionality shown in Figure 2 suggests SERS data sets can be used to selectively detect molecules in hyperspectral maps. We have previously reported the similarity between SERS spectra from aggregated GNPs and the spectra obtained from TERS detection of functionalized GNPs.[16, 18] In order to take advantage of multivariate regression of our data, we used partial least-squares discriminant analysis (PLS-DA) to determine the identity of components in our TERS imaging. PLS-DA calculates the spectral variance between validation/prediction set and calibration/training set, and assigns each sample to different classes.
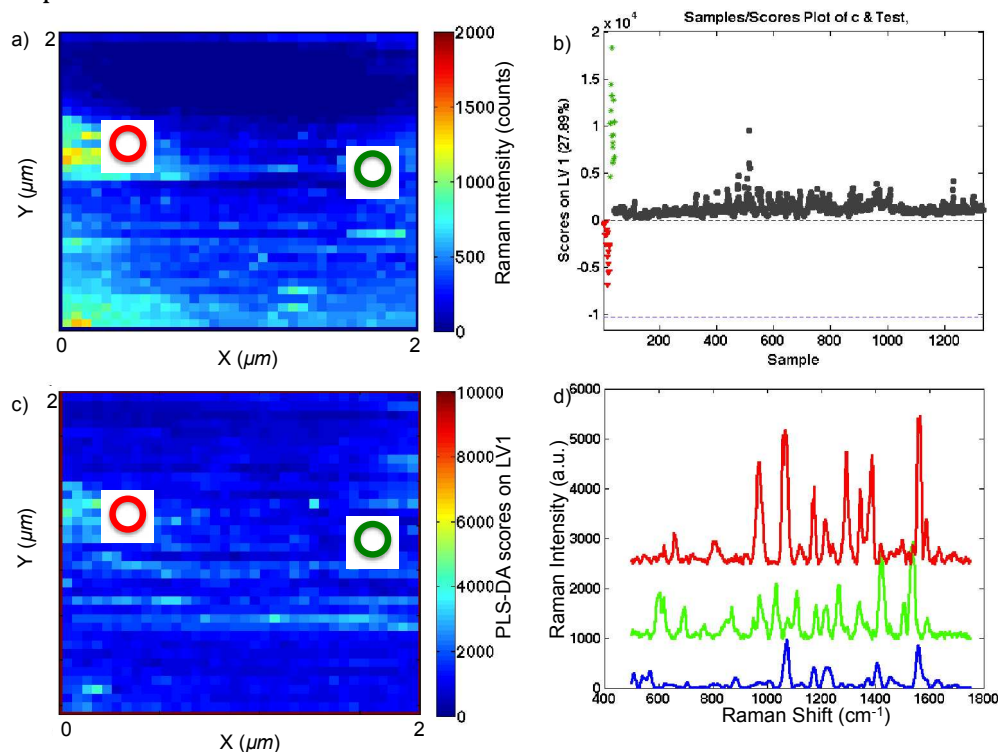
Figure 3. a) A 2x2 μm (36x36 pixel) TERS map at 960 cm⁻¹ is shown from 50nm streptavidin GNPs on biotinylated slide. b) Sample/scores are plotted against LV1 in PLS-DA analysis. The green and red data points are calibration SERS spectra of streptavidin and biotin, respectively. c) The PLS-DA calculated scores on LV1 are mapped as an indicator of the full-spectral similarity of each TERS spectrum to LV1. d) Selected TERS spectra are compared with PLS-DA calculated LV1 (blue); the green spectrum corresponds to TERS pixel circled in green and red spectrum corresponds to TERS pixel circled in red.

Figure 3 shows the use of plotting PLS-DA scores to improve image contrast for a specific chemical component. In Figure 3a, the TERS map obtained from streptavidin functionalized GNPs detected by a TERS tip is plotted using a single intense marker band (960cm⁻¹) to signify the detection of streptavidin GNPs. Using the PLS-DA model generated from the SERS spectra of biotin and streptavidin as the calibration set (39 spectra as in MCR model), we can calculate the score of each spectrum in the TERS map (1296 spectra) against the latent variable associated with streptavidin (LV1). Reconstructing the TERS map based on the scores of each TERS spectrum, we obtain an image with much better

contrast (Figure 3c). The multivariate analysis removes background signals not statistically similar to streptavidin but apparent in the single frequency intensity map.

A comparison in Figure 3d between the selected pixels in the TERS map and the PLS-DA calculated LV1 illustrates how PLS-DA recognizes streptavidin by taking into account the full spectrum in calculating variances: the green spectrum shows intensity that appears to be streptavidin when plotting single band intensities, but does not show agreement with LV1 in the reconstructed scores map while the red spectrum is retained due to its increased correlation to the spectrum of the pure component.
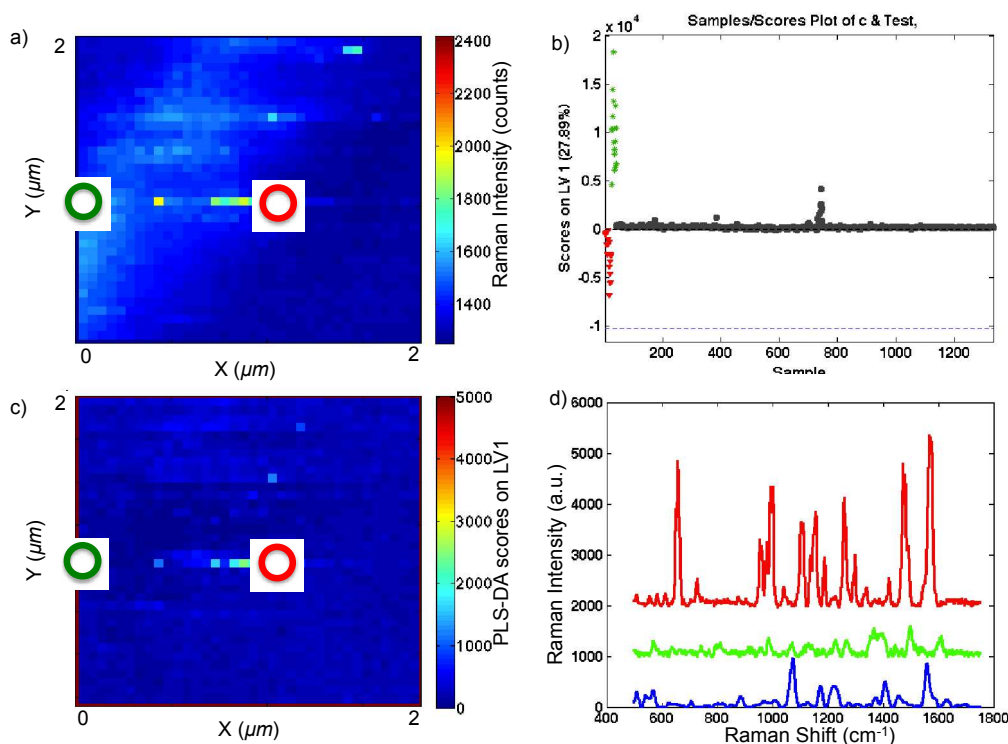
Figure 4. a) A 2x2 μm (36x36 pixel) TERS map at 960cm^{-1} is shown from 80nm biotinylated GNPs on streptavidin slide. b) Sample/scores are plotted against LV1 in PLS-DA analysis The green and red data points are calibration SERS spectra of streptavidin and biotin, respectively. c) The PLS-DA calculated scores on LV1 are mapped as an indicator of the full-spectral similarity of each TERS spectrum to LV1. d) Selected TERS spectra are compared with PLS-DA calculated LV1 (blue). The green spectrum corresponds to TERS pixel circled in green and red spectrum corresponds to TERS pixel circled in red.

To further assess PLS-DA score mapping to analyze TERS maps, we used the model to evaluate a sample with biotin functionalized GNPs on a streptavidin coated glass slide. Unlike the previous example where streptavidin resides between the GNPs and the TERS tip, in Figure 4 the streptavidin is located underneath the biotinylated GNPs. Comparing the Raman map (Figure 4a) through single band integration and the Raman map according to PLS-DA scores (Figure 4c), again we obtain better contrast. Figure 4d compares spectra comparison where even the highest scoring pixel (red) shows only a partial match with the calculated LV1 associated with streptavidin (blue), and again the random intense pixel (green) shows poor correspondence with the LV1 and is removed from analysis of the protein.

Interestingly, the PLS-DA scores from the biotinylated GNPs on a streptavidin slide are lower than the PLS-DA scores using streptavidin functionalized GNPs on a biotinylated surface. The scores calculated by PLS-DA for the streptavidin-GNPs (Figure 3) show a maximum around 10,000, while the score for the streptavidin detected beneath biotinylated GNPs only reach 5000 (Figure 4). The differences in PLS-DA scores suggest differences in enhancement related to the plasmonic environments experienced by the streptavidin protein and biotin ligands around the nanoparticles.

Large fields are expected in the gap region, which is likely where the protein resides in Figure 3. However, in Figure 4 where the protein is beneath the probe nanoparticle, the electric fields around the constructed dimer generate a lower level of scattering. One explanation for this is the redistribution of the electric fields arising from quantum tunneling effects.[23] The biotin coating may not keep the TERS tip from close (< 1 nm) contact with the nanoparticle.[22] In this regime, it has been reported that the gap mode is quenched, but fields exist around the dimer construct. This quenching may explain the diminished signal from biotin observed in these experiments. Alternatively, the observed signals may arise from changes in the plasmon resonances as the distance between the functionalized GNP and the TERS tip change.[33]

In addition to changes in the electric field distribution, the gradient of the electric field can also explain spectroscopic differences. When the streptavidin is between GNP and the TERS tip (e.g. Figure 3), the streptavidin signals is observed clearly and therefore scoring high on LV1. It is worth noting that streptavidin is a few nanometers in size and would inhibit the TERS tip from coming close enough to enter the quantum-tunneling regime. When biotinylated GNP resides on top of streptavidin, amino acids in the binding pocket of streptavidin and a small signal from biotin are observed.[16, 17] It should be noted that the biotin is attached to the GNP through a flexible linker, which makes the exact distance between the GNP, the TERS tip, and the biotin-streptavidin binding uncertain. However, in this case the detected signal contains contributions from both biotin and streptavidin indicating protein resides near the GNP surface. In experiments with antibody functionalized GNPs, the binding partner could not be detected.[15]

We previously postulated that the electric field gradients noted above give rise to signals associated with amino acids in the protein's binding pocket.[17] To assess the selectivity of PLS-DA mapping for discerning minor changes in protein composition and structure, here we investigated streptavidin mutants using biotinylated GNPs and TERS detection. The mutants included in the study have the substitutions listed in Table 1. In addition to the mutations, these proteins have a His-tag (MGSSHHHHHHS) attached for purification but that can also interact with GNP probes. Of particular note, tryptophan residue near the binding pocket is mutated in M5, which does not significantly alter its affinity for biotin.[29]

Table 1. Amino Acid Sequence of Streptavidin mutants

WT	MGSSHHHHHHSQDLASDPSKDSKAQVSAAEAGITGTWYNQLGSTFIVTAGAD GALTGTYESAVGNAESRY**V**LTGRYDSAPATDGSGTALGW**T**VAWKNNYRNAH SATTWSGQYVGGAEARINTQW**L**LTSGTTEANA**W**KSTL**V**GHDTFTKVKPSAA SGSDYKDDDDK
M5	MGSSHHHHHHSQDLASDPSKDSKAQVSAAEAGITGTWYNQLGSTFIVTAGAD GALTGTYESAVGNAESRY**T**LTGRYDSAPATDGSGTALGW**R**VAWKNNYRNAH SATTWSGQYVGGAEARINTQW**T**LTSGTTEANA**A**KSTL**R**GHDTFTKVKPSAA SGSDYKDDDDK
TMC	MGSSHHHHHHSQDLASDPSKDSKAQVSAAEAGITGTWYNQLGSTFIVTAGAD GALTGTYESAVGNAESRY**T**LTGRYDSAPATDGSGTALGW**R**VAWKNNYRNAH SATTWSGQYVGGAEARINTQW**T**LTSGTTEANA**W**KSTL**C**GHDTFTKVKPSAA SGSDYKDDDDK
RC	MGSSHHHHHHSQDLASDPSKDSKAQVSAAEAGITGTWYNQLGSTFIVTAGAD GALTGTYESAVGNAESRY**V**LTGRYDSAPATDGSGTALGW**R**VAWKNNYRNAH SATTWSGQYVGGAEARINTQW**L**LTSGTTEANA**W**KSTL**C**GHDTFTKVKPSAA SGSDYKDDDDK
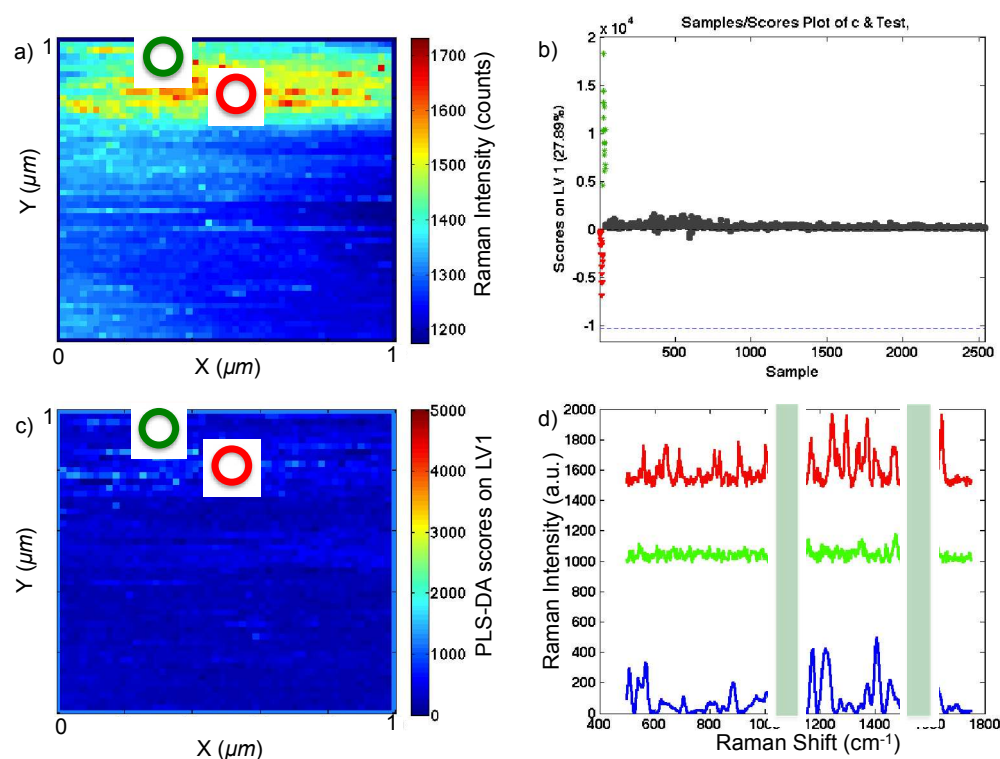
Figure 5. a) A 1x1 μm (50x50 pixel) TERS map at 960cm⁻¹ is shown from50nm biotinylated GNPs on M5-streptavidin slide. b) Sample/scores are plotted against LV1 in PLS-DA analysis. The green and red data points are calibration SERS spectra of streptavidin and biotin, respectively. c) The PLS-DA calculated scores on LV1 are mapped as an indicator of the full-spectral similarity of each TERS spectrum to LV1. d) Selected TERS spectra are compared with PLS-DA calculated LV1 (blue). The green spectrum corresponds to TERS pixel circled in green and red spectrum corresponds to TERS pixel circled in red.

Figure 5 is the TERS analysis obtained from biotinylated GNPs and the M5 mutant bound to a glass slide. While TERS maps show signals from the nanoparticle probe, the PLS-DA indicates it is not statistically similar to the native streptavidin (Figure 5b, c). Using single Raman band integration (Figure 5a), signals are observed, but the origin is difficult to discern. The TERS spectra shown in Figure 4d, red and green as circled in Figure 5a bear very little resemblance to the calculated LV1. Most prominently, a strong band at 1560 cm^{-1} is missing, which is consistent with tryptophan mutation to alanine in the M5 mutant.

Figure 6 shows the TERS mapping to the TMC mutant, which retains the tryptophan in the binding pocket and leads to a recovery of the PLS-DA score associated with streptavidin in the model (Figure 6b). By comparing Figure 6a and 6c, it is clear that the reconstructed Raman map with PLS-DA scores on LV1 exhibits improved accuracy in class assignment of each TERS spectrum. The spectra plotted in Figure 6d compares the high scoring and low scoring pixels, which can be easily confused as the same in Figure 6a, and reveals the prowess of PLS-DA in spectral pattern recognition. Similar to the TMC mutant, the other two recombinant streptavidin proteins that retained the tryptophan residue, wild type and the RC-mutant, showed PLS-DA scores indicating the detection of streptavidin (see Figure S2, S3 in the supporting information). Worth noting is the PLS-DA scores of the TMC, RC, and recombinant wild type are comparable to the native streptavidin in Figure 4. Because M5 is known to retain its affinity for biotin, the lack of PLS-DA scores for streptavidin suggests the tryptophan near the binding pocket makes an important contribution to TERS response from functionalized GNPs.
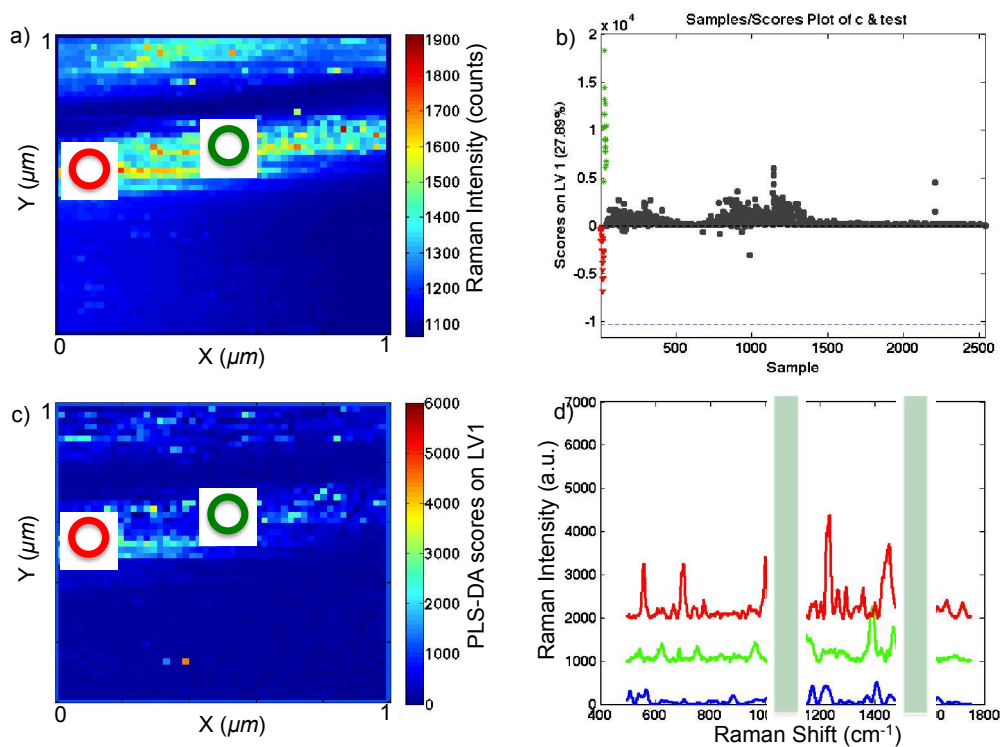
Figure 6. a) A 1x1 μm (50x50 pixel) TERS map at 960cm^{-1} of 50nm biotinylated GNPs on TMC-streptavidin slide is shown. b) Sample/scores are plotted against LV1 in the PLS-DA analysis. The green and red data points are calibration SERS spectra of streptavidin and biotin, respectively. c)

The PLS-DA calculated scores from LV1 are mapped as an indicator of the full-spectral similarity of each TERS spectrum to LV1. d) Selected TERS spectra are compared with PLS-DA calculated LV1 (blue). The green spectrum corresponds to TERS pixel circled in green and red spectrum corresponds to TERS pixel circled in red.

To assess the ability to selectively detect a specific biomolecule in a complex matrix, we applied this analysis to previously reported results from cyclo-arginine-glycine-aspartic acid-phenylalanine-cysteine (cRGD) peptides on GNPs bound to $\alpha_v\beta_3$ integrin receptors in intact cell membranes.[18] The PLS-DA model was produced from SERS spectra from the cRGD peptide and purified integrin detected in aggregated GNPs (Figure S4 in the supporting information). This model was then applied to TERS spectra generated by TERS mapping of RGD functionalized GNP on fixed cells.
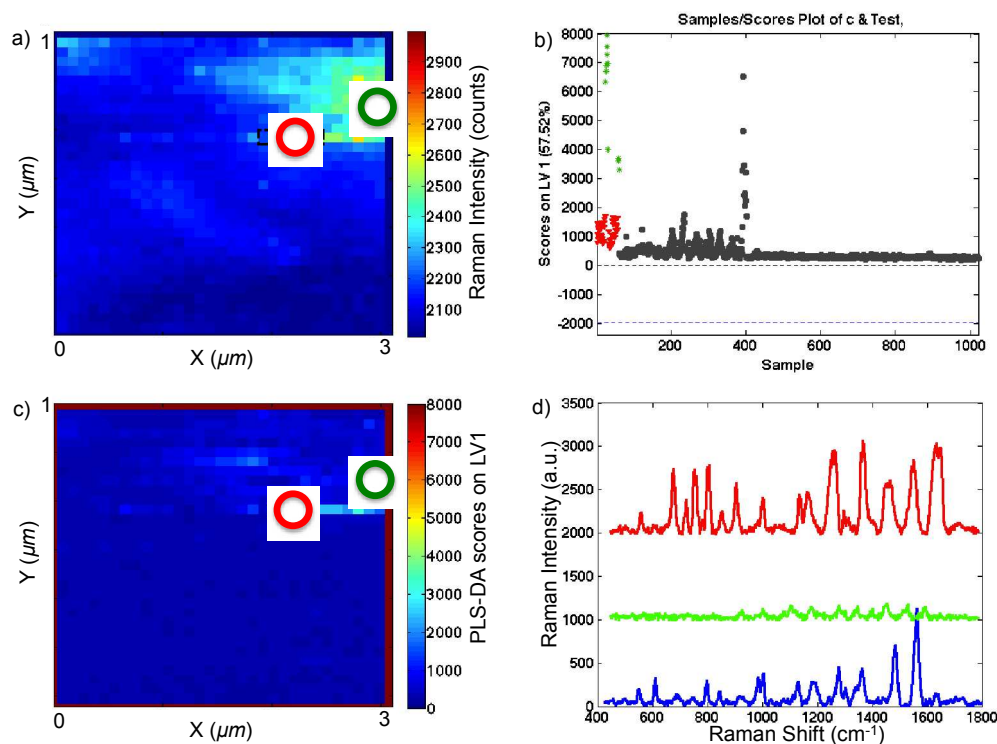
Figure 7. a) A 3x3 μm (31x31 pixel) TERS map at 1003cm^{-1} of RGD GNPs on SW620 cells is shown. b) The sample/scores are plotted against LV1 in the PLS-DA analysis. The green and red points are the calibration spectra from the integrin and RGD on GNPs, respectively. c) Scores map shows the PLS-DA calculated scores on LV1 as an indicator of the full-spectral similarity of each TERS spectrum to LV1. d) Selected TERS spectra are compared with the PLS-DA calculated LV1 (blue). The green spectrum corresponds to TERS pixel circled in green and red spectrum corresponds to TERS pixel circled in red.

Figure 7a shows the TERS map created by integrating the detected Raman band at 1003 cm^{-1}, which corresponds to a phenylalanine residue on the cRGD peptide. The PLS-DA scores on LV1 (Figure 7b) show pixels with statistical similarity, which in this case correlates to the SERS spectrum of the purified integrin receptor. The PLS-DA map (Figure 7c), again, improves contrast and enables locating the bound integrin on the cell membrane. The performance and utility of PLS-DA mapping is further illustrated through analysis of additional TERS maps in the supporting information (Figure S5).

The analysis done on streptavidin mutants shows how key amino acid differences can alter the observed signal. This suggests targeted nanoparticles

have utility for identifying receptors that bind specific ligands. The observed TERS signal in these experiments can provide information that, for example, may differentiate binding to the $\alpha_v\beta_3$ integrin versus one of the other 22 integrins in the cell membrane. This would be a powerful tool for investigating drug targeting and signaling pathways.

Our experience with TERS detection of ligand-functionalized nanoparticles indicates the detected signal arises overwhelmingly from the targeted protein receptor. In the case where the protein is functionalized to the probe-nanoparticle, the electric field gradient does not extend beyond the protein and the enhancement observed appears to arise from the protein in the gap.[15] However, with small molecule ligands the observed signal appears to arise from the targeted protein. This selectivity suggests that only the receptor is within the enhancing region of the electric field around the nanostructures. Recently we showed that physical confinement near the enhancing surfaces is important for SERS detection.[34] This seems to also be involved in enhancing the TERS signal. Interestingly, the ligand-receptor interactions are non-covalent bonds which further implicates physical confinement is important but not a direct chemical interaction.

Additionally, the magnitude of the PLS-DA score may provide information relevant to receptor clustering. The score from multivariate analysis can be calibrated to provide information on whether one or more receptors are being detected. In the case of integrins, clustering is reported to play a significant role in its signal transduction mechanism.[35] Differences in the observed PLS-DA score from an isolated nanoparticle may provide insight into multiple receptors clustering on a single nanoparticle that can be compared with receptors binding to multiple nanoparticles in a cluster. Additional work may provide new insight into this important biological receptor.

CONCLUSIONS:

The data presented illustrate the selectivity obtained from binding a functionalized nanoparticle to a protein receptor and detection with TERS. Using reference spectra obtained from SERS on purified biomolecules, the location of the biomolecule in a complex matrix can be imaged by TERS and background interference can be removed using PLS-DA. The regression analysis enables accurate identification and improved image contrast. Differences in the observed scores suggest different electromagnetic field environments may be responsible for the observed signals. Further analysis of the images may facilitate understanding of the plasmonic environments that generate the observed TERS signals.   Using protein mutants, it is clear that the amino acids involved in binding, specifically tryptophan, contribute significantly to the observed TERS signal. The approach presented takes advantage of controlled plasmonic interactions to enable highly selective detection. This may further elucidate the chemistry of ligand binding to protein receptors and other chemical recognition events in complex matrices.

ACKNOWLEDGEMENTS:

REFERENCES:

1. Z. D. Schultz, J. M. Marr and H. Wang, *Nanophotonics*, 2014, **3**, 91-104.
2. M. D. Sonntag, J. M. Klingsporn, A. B. Zrimsek, B. Sharma, L. K. Ruvuna and R. P. Van Duyne, *Chemical Society Reviews*, 2014, **43**, 1230-1247.
3. M. Moskovits, *The Journal of Chemical Physics*, 1978, **69**, 4159-4161.
4. P. Negri, R. J. Flaherty, O. O. Dada and Z. D. Schultz, *Chem. Commun.*, 2014, **50**, 2707-2710.
5. K. Kneipp, Y. Wang, H. Kneipp, L. T. Perelman, I. Itzkan, R. Dasari and M. S. Feld, *Phys. Rev. Lett.*, 1997, **78**, 1667-1670.
6. R. Zhang, Y. Zhang, Z. C. Dong, S. Jiang, C. Zhang, L. G. Chen, L. Zhang, Y. Liao, J. Aizpurua, Y. Luo, J. L. Yang and J. G. Hou, *Nature*, 2013, **498**, 82-86.
7. R. M. Stockle, Y. D. Suh, V. Deckert and R. Zenobi, *Chem Phys Lett*, 2000, **318**, 131-136.
8. N. Hayazawa, Y. Inouye, Z. Sekkat and S. Kawata, *Optics Communications*, 2000, **183**, 333-336.
9. J. Steidtner and B. Pettinger, *Phys. Rev. Lett.*, 2008, **100**.
10. K. L. Wustholz, A.-I. Henry, J. M. McMahon, R. G. Freeman, N. Valley, M. E. Piotti, M. J. Natan, G. C. Schatz and R. P. V. Duyne, *J. Am. Chem. Soc.*, 2010, **132**, 10903-10910.
11. M. Richter, M. Hedegaard, T. Deckert-Gaudig, P. Lampen and V. Deckert, *Small*, 2011, **7**, 209-214.
12. R. Bohme, M. Richter, D. Cialla, P. Rosch, V. Deckert and J. Popp, *Journal of Raman Spectroscopy*, 2009, **40**, 1452-1457.
13. U. Neugebauer, P. Rosch, M. Schmitt, J. Popp, C. Julien, A. Rasmussen, C. Budich and V. Deckert, *ChemPhysChem*, 2006, **7**, 1428-1430.
14. P. Olk, J. Renger, T. Hartling, M. T. Wenzel and L. M. Eng, *Nano Lett*, 2007, **7**, 1736-1740.
15. K. D. Alexander and Z. D. Schultz, *Anal Chem*, 2012, **84**, 7408-7414.
16. H. Wang and Z. D. Schultz, *Analyst*, 2013, **138**, 3150-3157.
17. S. L. Carrier, C. M. Kownacki and Z. D. Schultz, *Chem. Commun.*, 2011, **47**, 2065-2067.
18. H. Wang and Z. D. Schultz, *ChemPhysChem*, 2014 IN PRESS, **DOI: 10.1002/cphc.201402466R1**.
19. E. Hao and G. C. Schatz, *J Chem Phys*, 2004, **120**, 357-366.
20. L. K. Ausman and G. C. Schatz, *J Chem Phys*, 2009, **131**, 10.
21. K. A. Willets, S. M. Stranahan and M. L. Weber, *J. Phys. Chem. Lett.*, 2012, **3**, 1286-1294.
22. R. Esteban, A. G. Borisov, P. Nordlander and J. Aizpurua, *Nat. Commun.*, 2012, **3**.
23. T. V. Teperik, P. Nordlander, J. Aizpurua and A. G. Borisov, *Optics Express*, 2013, **21**, 27306-27325.
24. L. Chuntonov and G. Haran, *Nano Lett*, 2011, **11**, 2440-2445.
25. T. Shegai, Z. P. Li, T. Dadosh, Z. Y. Zhang, H. X. Xu and G. Haran, *Proc. Natl. Acad. Sci. U. S. A.*, 2008, **105**, 16448-16453.

26. N. J. Halas, S. Lal, W. S. Chang, S. Link and P. Nordlander, *Chem. Rev.*, 2011, **111**, 3913-3961.
27. J. Ye, F. F. Wen, H. Sobhani, J. B. Lassiter, P. Van Dorpe, P. Nordlander and N. J. Halas, *Nano Lett.*, 2012, **12**, 1660-1667.
28. K. D. Alexander, K. Skinner, S. P. Zhang, H. Wei and R. Lopez, *Nano Lett*, 2010, **10**, 4488-4493.
29. K. H. Lim, H. Huang, A. Pralle and S. Park, *Biochemistry*, 2011, **50**, 8682-8691.
30. Z. D. Schultz, S. J. Stranick and I. W. Levin, *Anal. Chem.*, 2009, **81**, 9657-9663.
31. Z. D. Schultz, S. J. Stranick and I. W. Levin, *Appl. Spectrosc.*, 2008, **62**, 1173-1179.
32. D. Graham, R. Stevenson, D. G. Thompson, L. Barrett, C. Dalton and K. Faulds, *Faraday Discuss.*, 2011, **149**, 291-299.
33. J. D. Driskell, R. J. Lipert and M. D. Porter, *The journal of physical chemistry. B*, 2006, **110**, 17444-17451.
34. S. M. Asiala and Z. D. Schultz, *Anal. Chem.*, 2014, **86**, 2625-2632.
35. E. Ruoslahti, *Annual review of cell and developmental biology*, 1996, **12**, 697-715.